Remote Sensing of Environment 143 (2014) 15–25

Contents lists available at ScienceDirect

Remote Sensing of Environment

journal homepage: www.elsevier.com/locate/rse

Sensitivity of direct canopy gap fraction retrieval from airborne waveform lidar to topography and survey characteristics

X.T. Chen [a], M.I. Disney [b,c,*], P. Lewis [b,c], J. Armston [d,e], J.T. Han [a], J.C. Li [a]

[a] College of Electronic Science and Engineering, National University of Defense Technology, 137 Yanwachi, Changsha, Hunan 410073, PR China
[b] Dept. of Geography, University College London, Gower Street, London WC1E 6BT, UK
[c] NERC National Centre for Earth Observation (NCEO), UK
[d] Remote Sensing Centre, Science Delivery, Department of Science, Information Technology, Innovation and the Arts, 41 Boggo Road, QLD 4102, Australia
[e] Joint Remote Sensing Research Program, School of Geography, Planning and Environmental Management, University of Queensland, St Lucia, QLD 4072, Australia

ARTICLE INFO

Article history:
Received 30 September 2013
Received in revised form 16 December 2013
Accepted 17 December 2013
Available online 15 January 2014

Keywords:
Waveform lidar
Canopy
Gap fraction
Airborne
Forest
Biophysical parameters

ABSTRACT

Recently, Armston et al. (2013) have demonstrated that a new, physically-based method for direct retrieval of canopy gap probability P_{gap} from waveform lidar can improve the estimation of P_{gap} over discrete return lidar data. The success of the approach was demonstrated in a savanna woodland environment in Australia. The huge advantage of this method is that it uses the data themselves to solve for the canopy contrast term i.e. the ratio of the reflectance from crown and ground, ρ_v/ρ_g. In this way the method avoids local calibration that is typically required to overcome differences in either ρ_v or ρ_g. To be more generally useful the method must be demonstrated on different sites and in the presence of slope and different sensor and survey configurations. If it is robust to these things, slope in particular, then we would suggest it is likely to be widely useful. Here, we test the robustness of the retrieval of P_{gap} from waveform lidar using the Watershed Allied Telemetry Experimental Research dataset, over the Heihe River Basin region of China. The data contain significant canopy, terrain and survey variations, presenting a rather different set of conditions to those previously used. Results show that ρ_v/ρ_g is seen to be stable across all flights and for all levels of spatial aggregation. This strongly supports the robustness of the new P_{gap} retrieval method, which assumes that this relationship is stable. A comparison between P_{gap} estimated from hemiphotos and from the waveform lidar showed agreement with Pearson correlation coefficient $R = 0.91$. The waveform lidar-derived estimates of P_{gap} agreed to within 8% of values derived from hemiphotos, with a bias of 0.17%. The new waveform model was shown to be stable across different off-nadir scan angles and in the presence of slopes up to 26° with $R \geq 0.85$ in all cases. We also show that the waveform model can be used to calculate P_{gap} using just the mean value of canopy returns, assuming that their distribution is unimodal. Lastly, we show that the method can also be applied to discrete return lidar data, albeit with slightly lower accuracy and higher bias, allowing P_{gap} comparisons with previously-collected lidar datasets. Our results show the new method should be applicable for estimating P_{gap} robustly across large areas, and from lidar data collected at different times and using different systems; an increasingly important requirement.

1. Introduction

Directional gap probability, $P_{gap}(\theta)$, is defined as the probability of a light beam of infinitesimal width at zenith angle θ to the local normal, being directly transmitted through a vegetation canopy (Armston et al., 2013). $P_{gap}(\theta)$, along with canopy height and leaf area index (LAI), are some of the most important forest structural parameters used to directly interpret the transfer of radiation, carbon, and related processes in physical systems (Ross, 1981; Verstraete, Pinty, & Myneni, 1996). $P_{gap}(\theta)$ is equivalent to the probability that the ground surface is directly visible from an airborne or spaceborne lidar remote sensing instrument. As a consequence, $P_{gap}(\theta)$ is a structural parameter that may be near-directly retrieved from airborne lidar measurements (Ni-Meister, Jupp, & Dubayah, 2001).

The importance of $P_{gap}(\theta)$ is its relationship to radiation interception within the canopy and hence other canopy structure parameters, like LAI and above-ground biomass (Campbell & Norman, 1989; Ni-Meister et al., 2010). These latter properties may be modelled using different expressions, combinations or spatial variance of canopy height and $P_{gap}(\theta)$, since the $P_{gap}(\theta)$ represents the integrated effect of several scale-dependent canopy structural properties (in particular LAI and leaf

* Corresponding author at: Dept. of Geography, University College London, Gower Street, London WC1E 6BT, UK. Tel.: +44 20 7679 0592.
E-mail addresses: chenxiaotian@nudt.edu.cn (X.T. Chen), mathias.disney@ucl.ac.uk (M.I. Disney), p.lewis@ucl.ac.uk (P. Lewis), John.Armston@science.dsitia.qld.gov.au (J. Armston), hanjt@nudt.edu.cn (J.T. Han), peter0516@126.com (J.C. Li).

0034-4257
http://dx.doi.org/10.1016/j.rse.2013.12.010

angle distribution, LAD). In practice, $P_{gap}(\theta)$ is often calculated over a narrow range of angles e.g. close to nadir ($\theta = 0°$) and is then referred to simply as P_{gap}. Here, we refer to P_{gap} and note where there may be some angular dependence.

Many studies have estimated P_{gap} or fractional cover (1- P_{gap}) using small footprint discrete return lidar datesets (Hopkinson & Chasmer, 2009; Liu et al., 2008; Lovell, Jupp, Culvenor, & Coops, 2003). Quantifying the proportion of lidar pulses intercepted by the canopy is the most common method to estimate the P_{gap} (Lovell et al., 2003). There are two problems in discrete return approaches to estimate P_{gap} (Armston et al., 2013): firstly, parameters estimated based on discrete return lidar returns are only 'effective', i.e. they only have indirect correspondence with a physically-measurable estimate of the same parameter which means that they are difficult to validate and interpret; secondly, discrete return lidar approaches tend to rely on site-, sensor- and survey-specific calibrations, which limits the application of such methods in larger areas. In particular, topography and scan angle (as well as other things such as sensor flying height and even canopy structure and crown shape) combine in practice to modify the lidar return by changing the size and shape of the footprint and the path length through the canopy and hence the returned energy. These factors can introduce significant bias into estimates of properties derived from the footprint, even in 'simple' metrics such as canopy height. Disney et al. (2010) used detailed 3D Monte Carlo ray tracing to study the impact of footprint size, scan angle and crown shape (among other things) on small footprint (<1 m) discrete return lidar estimates of canopy height, showing that these factors could lead to large over- or underestimates depending on the situation. Yang, Ni-Meister, and Lee (2011) used a geometric-optics radiative transfer (GORT) model to explore the impact of topography, crown shape and scan angle on large footprint (>20 m) waveform lidar. They showed that the impact of topography and scan angle on waveform properties were similar and combined to smear out the returned waveform shape and reduce the energy returned with height through the canopy, potentially resulting in canopy height overestimates approaching 50%. Romanczyk et al. (2013) also showed that the impact of within-crown distribution of leaf and woody material on simulated waveform lidar returns varied with footprint and scan angles. All of these effects will also impact estimates of P_{gap}, typically by acting to reduce it if the path length through the canopy is increased by scan angle or topography (and vice versa).

Recently, a new method proposed by Armston et al. (2013) has demonstrated that a physically-based method for direct retrieval of P_{gap} from waveform lidar can improve the estimation of P_{gap} from airborne platforms compared to discrete return lidar data in a savanna woodland environment. The method assumes that the ratio of the canopy and ground reflectance characteristics, ρ_v and ρ_g respectively, is constant within a local area. The advantage of this method, is that if ρ_v/ρ_g is constant, then the method solves for the ratio term using the lidar waveforms themselves. Previous methods based on the properties of ρ_v/ρ_g have tended to require some estimate of either ρ_g or ρ_v to constrain the ratio (e.g. Lefsky, Hudak, Cohen, & Acker, 2005). Hence the method of Armston et al. (2013) does not rely on local calibration that is typically required to overcome differences in either ρ_v or ρ_g. As a result it is less sensitive to possible changes in lidar system gain and instrument altitude. This makes the method much more applicable for large scale and/or repeat applications, where system and survey characteristics are very hard to replicate (or potentially even determine).

Armston et al. (2013) showed that the assumption of constant ρ_v/ρ_g held very well for the cases they explored and produced estimates of P_{gap} corresponding to within 5% of ground measurements. They also showed that the resulting P_{gap} estimates were relatively insensitive to variations in sensor altitude, in contrast to other methods, where altitude variations can result in changes of up to 15% in estimated P_{gap}.

Crucially, if it can be demonstrated that the assumptions of stable ρ_v/ρ_g holds across different sets of sensor, survey, and canopy structure configurations than in the original study, and in contrasting environments, this would provide further evidence that the method is more generally applicable. Additional validation of the method in different environments is needed to demonstrate that a reduction or even removal of the requirements for local field calibration is justified, which in turn would advance the wider application of airborne waveform lidar for estimating P_{gap}.

Here, we examine the physically-based method for direct retrieval of P_{gap} from waveform lidar over a mountainous conifer forest region in the Heihe River Basin region of China (Li et al., 2009). We use airborne waveform lidar data containing a range of system variations (i.e. flying height, scanning angle, gain setting), over a survey area containing a range of different slopes and terrain types as well as a variation of tree type and density in a dense Picea forest environment (Tian et al., 2011). This extends validation of the stability of the assumption of ρ_v/ρ_g to a new environment, containing significant topography, as well as different canopy density and crown shape to those of Armston et al. (2013). We also test the P_{gap} retrieval method using a discrete return lidar dataset synthesised from the waveform data. This allows us to test whether the physically-based P_{gap} estimation method could also be applied to discrete return data. If so, this would make it widely-applicable to lidar datasets collected in the past with different sensor systems. This would be of wide use in many lidar applications, particularly those examining changes over time i.e. comparing lidar-derived estimates of gap fraction over time.

2. Data

2.1. Study site and field data

In this study we use an airborne lidar survey comprising six flights, combined with forest structure parameter survey data to test the retrieval of P_{gap}. The lidar data were collected on 23/06/2008 over the Dayekou watershed as part of the larger Watershed Allied Telemetry Experimental Research (WATER) project (Li et al., 2009). WATER covers the Heihe River Basin in Northwest China, the second largest inland river basin in China, located between 37.68–42.70°N and 97.4–102.17°E with an area of about 130,000 km^2. WATER is aimed at improving the understanding of physical processes of the land surface–atmosphere interaction in arid regions, and has resulted in the collection of simultaneous airborne, satellite-borne remote sensing observations and ground-based measurements. Fig. 1 shows the site location within China and a zoom on the map shows the coverage of the flight lines.

The so-called Dayekou Super Site is located at Xishui farm, Su'nan Yuguzu Autonomous County in the Gansu Qilian Mountains National Nature Reserve (38.53° N, 100.25° E). The site is a water resource conservation forest in the Dayekou Basin of the Qilian Mountains, and lies within the temperate alpine, cold semiarid and semi-humid zones, characterized by mountain forest-steppe (Li et al., 2009). Sunny slopes are covered with mountain grassland, and shady slopes are forested. The elevation ranges from 2700 to 3000 m above sea level, with mean elevation of ~2800 m. Fig. 2 shows the topographic features of the Super Site. There are four subplots in the test site (designated s_1–s_4). From the contours in Fig. 2, we see that s_4 has the highest gradient at about 15°. By contrast, s_1 has the lowest gradient in all the subplots. The topographic variation here is more complex than the savanna woodland environment used in Armston et al. (2013), providing a very different set of conditions to test the assumptions underlying the P_{gap} reconstruction method.

The forest cover across the Super Site is natural mature secondary forest dominated by Picea crassifolia Kom, and the forest floor is covered mainly with moss (*Carex lansuensis*, *Pedicularis muscicola*, *Polygonum viviparum*). An inventory survey on the forest has been carried out in the four subplots, including tree height (TH) and diameter at breast height (DBH). Histograms of these forest structure parameters are given in Fig. 3 (Liu, 2009) .

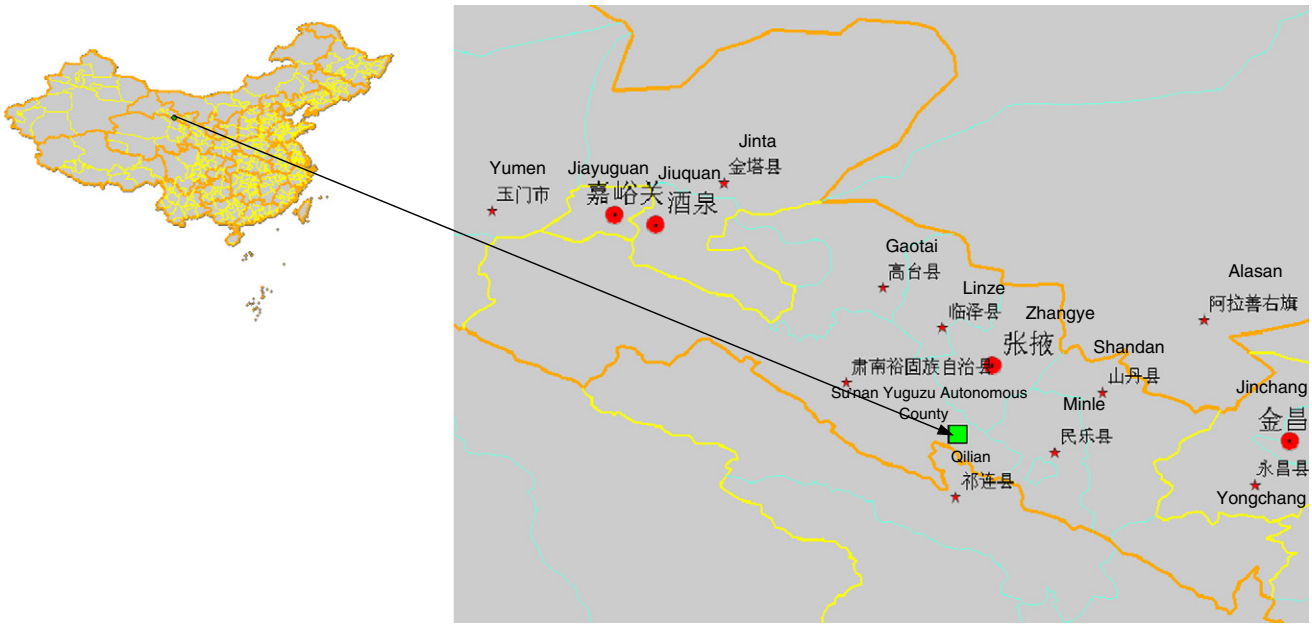

Fig. 1. Position sketch of Dayoukou Observation at water conversation forest in Qilian Mountain (source: Li et al., 2008) . The green box denotes the site of the lidar flights.

From the histograms of DBH in Fig. 3 (and their kurtosis and skewness parameters), it is clear that the smaller, less mature trees are more numerous than the mature trees. From the bimodal characteristics of the histogram of TH it seems that there are distinct layers in the structure of the forest canopy across the site. The higher part is composed of mature trees (>15 m), a lower part dominated by trees in the 5–15 m range, and a bottom layer of young growth trees (<5 m). From Fig. 4 the forest structure here is denser and more mixed in age, and located on significant slopes in places, contrasting with that used in Armston et al. (2013) which was dominated by sparse, mature trees on flat surfaces.

2.2. Field data

Hemiphotos were taken looking upwards from the forest floor in the supersite using a 180° fisheye lens (Canon EF15/28) and a high resolution digital camera (Canon EOS40D) (Chen & Guo, 2008; Chen, Guo, & Liu, 2008). The digital camera is mounted in a self-levelling Mount, type SLM9. Hemiphotos were taken when the sky was evenly overcast. 32 photographs taken from the subplots were analysed to provide estimates of P_{gap} (plus variation) of each subplot, using the HemiView canopy image analysis system (Delta T Devices, Cambridge, UK). We obtained P_{gap} from Hemiphotos measuring the directional gap probability at near-nadir i.e. zenith angles in the range 0–5°.

2.3. Lidar data

The lidar surveys used in this study were acquired using a Riegl LMS-Q560 full waveform scanner during 6 flights over 23/06/2008. Details of the acquisitions are shown in Table 1 (Pang et al., 2008). Data were acquired at flying heights of 700–750 m. The variation of elevation above sea level between the flights was from 3500 to 3550 m. Parallel flight tracks were designed to have 90% overlap to ensure a multi-angular airborne dataset over the field sites and nearly nadir angular (<15°) scanning of the site. The coverage and nominal height of all

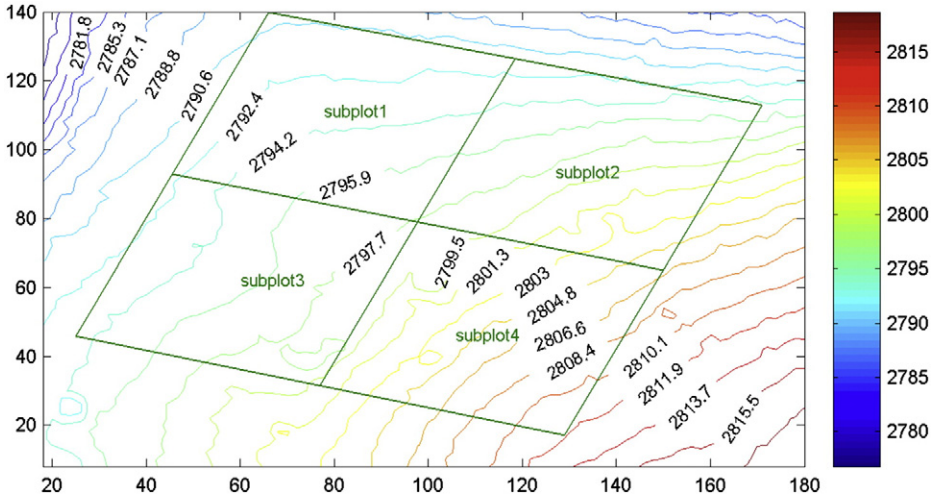

Fig. 2. Contours of the Dayoukou Super Site showing the locations of the subplots 1–4 using a local frame of reference (absolute origin 6.089×10^6, 4.2657×10^6).

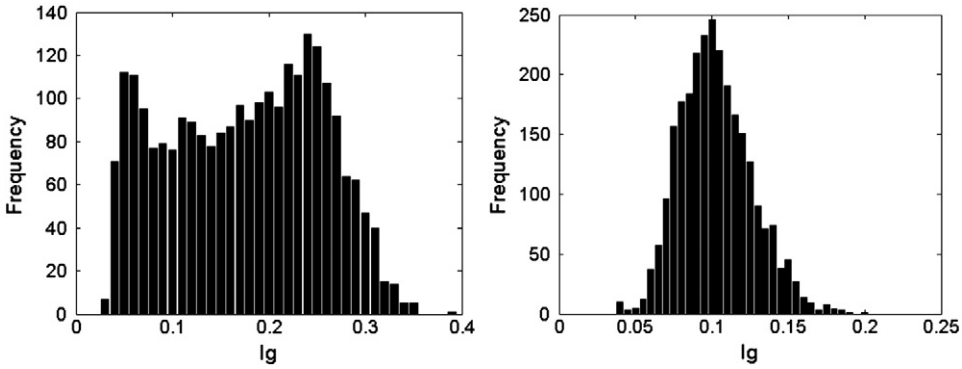

Fig. 3. Histograms of forest structure parameters measured in the Dayekou super site: tree height (left) and diameter-at-breast-height (right).

flights are shown in Fig. 4. The different scanning angles of each of the 6 flights over super site are also shown in Fig. 5.

3. Methods

3.1. Lidar data processing

For the Riegl LMS-Q560 airborne surveys, raw waveform data were made available (Riegl, 2008). These data were processed by Gaussian decomposition using the method described by Wagner, Ullrich, Ducic, Melzer, and Studnicka (2006). This resulted in Gaussian parameters according to Eq. (1):

$$R(t) = \epsilon + \frac{\sum_{i=1}^{N} A_i e^{\frac{(t-t_i)^2}{2\sigma_i^2}}}{N} \quad (1)$$

For each return R(t) at time t, ϵ is the noise level, a nominal value greater than background solar irradiance and photon counting noise contributions. A_i is the amplitude of Gaussian component i; t_i is the time (or range) and σ_i is the standard deviation of Gaussian component i.

The Reigl LMS-Q560 data also provided the LAS format dataset, which included the discrete return results detected from the received waveform (Riegl, 2008). An example of the full waveform and corresponding Gaussian-fitted result and discrete return values from the LMS-Q560 data used here are shown in Fig. 6.

3.1.1. Separating crown and ground returns in the lidar data

The airborne LIDAR data from the super site in the Dayekou watershed flight zone were used to generate a digital elevation model (DEM) (Liu, 2009), which was created by combining the six lidar flights described above. We also compared the agreement of the lidar-derived DEM with 1506 survey points measured by total station in the field. The mean and standard deviation of the difference between the lidar-derived and total station points were 0.23 m and 0.21 m respectively. In this case it is intuitive to separate crown returns from ground returns with an elevation threshold ($\Delta h = 0.5$ m) using the DEM data.

3.1.2. Comparison of topography and lidar survey characteristics

The dataset that we used to test the waveform model of P_{gap} includes different scan angles (lidar pointing direction, Yang et al., 2011), topography (slope), and flying height (albeit only small variations), which interact to affect pulse incidence angle, range, and footprint size, that in turn directly impact the lidar waveform. Here we make the assumption that the vegetation grows relative to the gravity normal and lidar measures relative to its pointing direction. We define the featured vegetation height H_0 as the distance from the top of the canopy to the ground along gravity normal, which could be measured by lidar as the 'distorted' (or projected) height H, defined as the distance from the first vegetation signal to the ground along the lidar pointing direction (Yang et al., 2011). The energy of return waveform is mainly affected by the range R between the lidar and surface objects. The change of waveform extent is caused by H, which changes with the footprint diameter F, pulse incidence angle γ, and terrain slope angle θ_p, which can be expressed in Eq. (2) (Yang et al., 2011):

$$H = \frac{H_0 \cos\theta_p}{\cos\gamma} + F\tan\gamma. \quad (2)$$

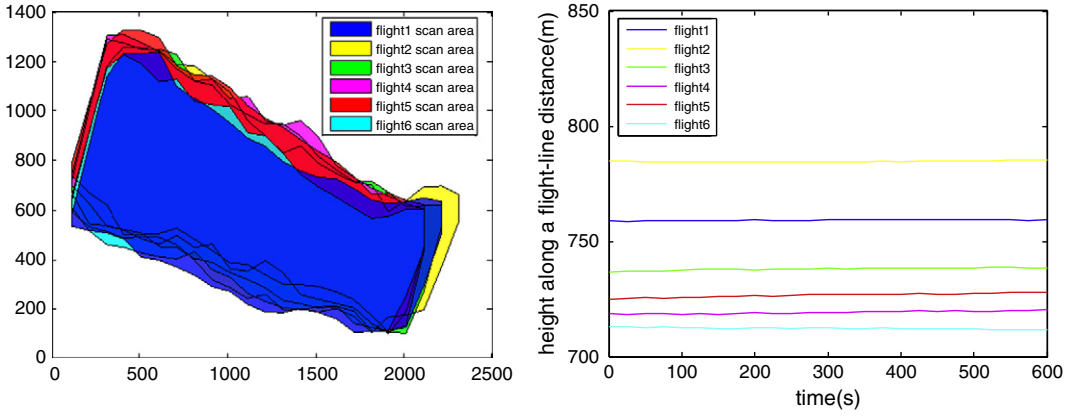

Fig. 4. The scanning area (left) and height of the six lidar flights along a normalised flight-line distance (right) (absolute origin 6.089×10^6, 4.2657×10^6).

Table 1
Lidar survey and sensor characteristics, for the Riegl LMS-Q560 sensor used in this study.

Wavelength (μm)	1550
Pulse length (ns)	3.5
Swath width (m)	700
Footprint diameter	38
Pulse rate (kHz)	100
Pulse density (m^{-2})	0.78
Nominal altitude	760
Max. zenith angle (°)	30

In Eq. (2), pulse incidence angle γ on the surface of terrain can be obtained from the terrain slope angle θ_p and laser pointing (scan) angle θ_i i.e.

$$\cos\gamma = \cos\theta_i \cos\theta_p + \sin\theta_i \sin\theta_p. \quad (3)$$

In Eq. (3), the azimuth angle of the lidar beam and slope are regarded as zero. This assumption is justified given that the flightlines were predominantly conducted up- or down-slope.

In Section 4.1 (survey 1), we use the super site data that includes four subplots where the mean slope is <9° and the lidar scan angle is within 5° so slight differences in waveform shape across the six flights was mainly caused by the range between the lidar and the surface objects. In Section 4.3 (survey 2), we show the result of impact of varying off-nadir scan angles (constant flying height) over the area where the slope is below 8°, so the difference in waveform was mainly caused by incidence angle which was nearly equal to the off-nadir scan angle according to Eq. (3). In Section 4.4 (survey 3), we compare the result of different slopes in the same flight with nadir scan angle. In this case the difference of the waveform is mainly caused by the terrain slope angle θ_p and incidence angle γ which was nearly equal to the slope angle θ_p according to Eq. (3). The variations in the distance to target (i.e. range) L and H in these three surveys are given in Fig. 7. For

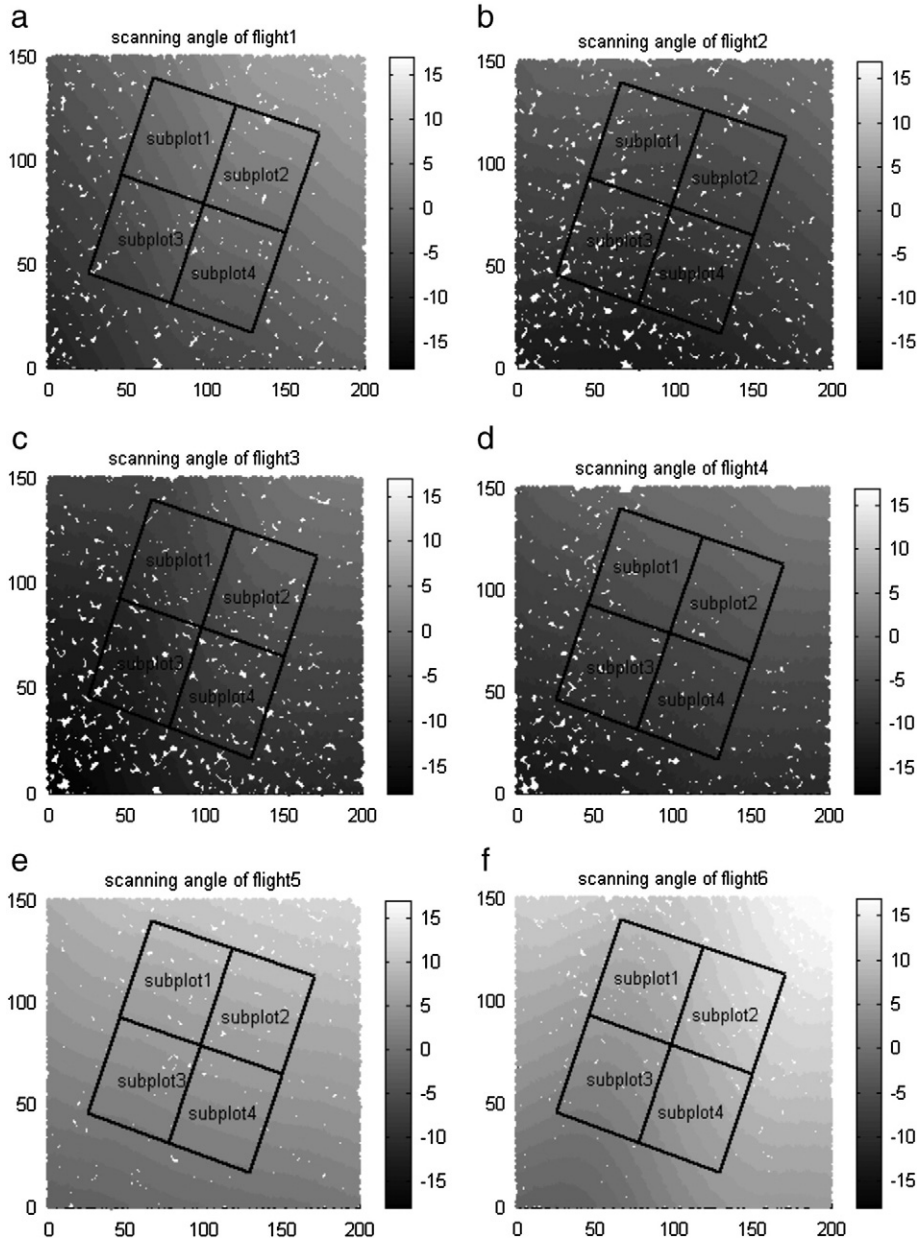

Fig. 5. Distribution of scanning angles of the lidar points over the site for each flight line (local coordinates in each case). Scan angles are grouped into 1° contours.

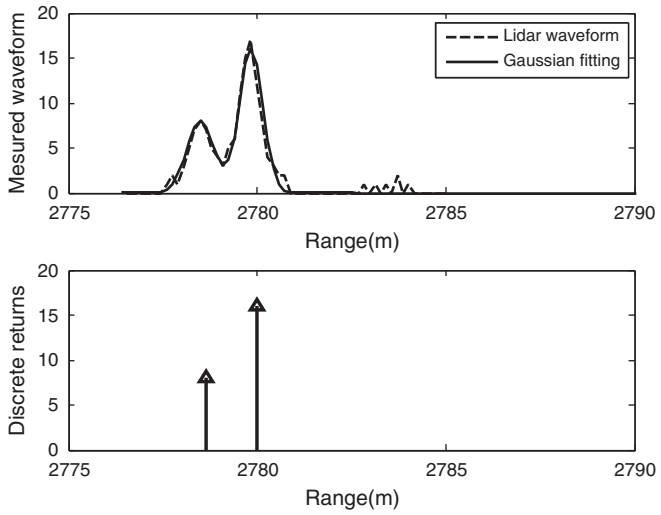

Fig. 6. Measured and corresponding Gaussian modelled raw waveform for a single Riegl LMS-Q560 pulse (top) and the corresponding discrete return signal (bottom).

the variation of H, H_0 was set by the mean height (8 m) of trees in the surveys.

3.2. Estimation of P_{gap}

In previous research using discrete return lidar, P_{gap} is typically estimated using some expression of the proportion of returns intercepted by the canopy within a height bin (Hopkinson & Chasmer, 2009; Liu et al., 2008; Lovell et al., 2003), which we refer to as the 'HIT' method. Here, we additionally tested this discrete return method for estimating P_{gap} in order to compare with the robust waveform method assuming constant ρ_v/ρ_g. This has two purposes: i) to enable us to quantify the advantage of waveform lidar data (if any) for estimating P_{gap} in this way; and ii) allowing a measure of 'backward compatibility' with discrete return datasets by exploring the reliability of the assumption of constant ρ_v/ρ_g derived from those data.

For the HIT method, we synthesised a discrete return dataset by aggregating first returns for each pulse, then taking the cumulative sum and normalising by the total number of pulses (N). The P_{gap} from above the canopy down to height z_i was then estimated as:

$$P_{gap}(z) = 1 - \frac{\sum_{z=z_i}^{z=\max(z)} \#z_i}{N}. \quad (4)$$

Then, we applied the nomenclature of Ni-Meister et al. (2001) to get P_{gap} from the waveform lidar data. The assumption here is that the lidar returns are dominated by first order scattering only (i.e. only one interaction of transmitted photons with ground or vegetation elements). In this case the total returned waveform energy R can be separated into independent vegetation and ground backscatter components:

$$R = R_v + R_g \quad (5)$$

where R_v is the integrated vegetation backscatter component of the waveform and R_g the integrated ground return. Assuming the recorded lidar signal is linearly related to the received power, P_{gap} can then be estimated from uncalibrated waveforms through Eq. (6) of Ni-Meister et al. (2001):

$$P_{gap}(z) = 1 - \frac{\sum_{z=z_i}^{z=\max(z)} R_{v,i}}{R_v} \frac{1}{1 + \frac{\rho_v}{\rho_g}\frac{R_g}{R_v}} \quad (6)$$

where ρ_v is the backscattering coefficient of vegetation, and ρ_g is the backscattering coefficient of the ground; $R_{v,i}$ is the integrated vegetation backscatter component of the waveform from the top of the canopy down to height z_i; R_g is the ground backscatter integral. R_v and R_g can be expressed as a function of P_{gap} (Armston et al., 2013):

$$R_g = J_0\, P_{gap}(0)\rho_g \quad (7)$$

$$R_v = J_0\, P_{gap}(0)\rho_v. \quad (8)$$

J_0 is the transmitted pulse energy corrected for transmission losses. By substituting P_{gap} from Eqs. (7) into (8) we can define a linear relationship between R_g and R_v:

$$R_g = J_0\, R_g - \frac{\rho_g}{\rho_v} R_v. \quad (9)$$

If we substitute the R_v from Eq. (9) into Eq. (6), we can obtain an alternative expression for P_{gap} (Armston et al., 2013):

$$P_{gap}(z) = 1 - \frac{\sum_{z=z_i}^{z=\max(z)} R_{v,i}}{R_v} \frac{1}{1 + \frac{R_g}{J_0\rho_g - R_g}}. \quad (10)$$

For Eq. (10), if $z_i = 0$, total canopy P_{gap} is independent of R_v as well as ρ_v. It also means that waveform estimates of P_{gap} may be calculated with only an estimate of $J_0\rho_g$. For small footprint waveform lidar, an estimate of $J_0\rho_g$ can easily be calculated as the mean integral of unimodal ground returns, assuming ρ_g is constant and the mean

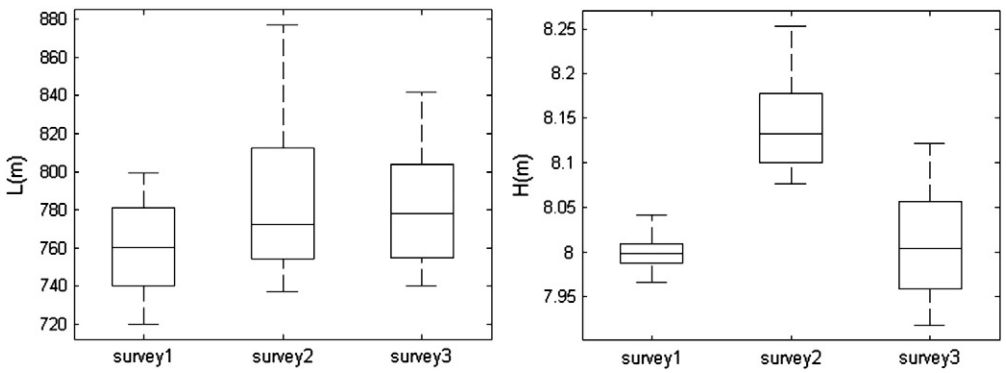

Fig. 7. The variation of range L (left) and projected canopy height H (right) in three surveys. The boxes in each case represent the second and third quartiles of each distribution about the mean. The upper and lower whiskers represent the range.

converges to a normal distribution. Conversely if the assumption of normal distribution of ρ_g is violated but the canopy returns follow a normal distribution and are unimodally distributed, we can substitute the R_g from Eq. (9) into Eq. (6) to express P_{gap} as:

$$P_{gap}(z) = 1 - \frac{\sum_{z=z_i}^{z=\max(z)} R_{v,i}}{R_v} \frac{R_v}{J_0 \rho_v}. \quad (11)$$

In Eq. (11) total canopy P_{gap} is calculated by $J_0\rho_v$, which can be calculated as the mean integral of unimodal canopy returns. This assumes that the integrated canopy returns are truly unimodal and there is clear distinction between the form and location (in height) of the crown and ground returns. Where the contrast between scattering from overstory and understory is relatively small and/or there is significant convolution of the returns from the (hard) ground and (soft) understory, this assumption will not hold and ρ_v is likely to be systematically underestimated. We discuss the implications of this below.

In this study, we calculated waveform estimates of P_{gap} using the Gaussian amplitudes and standard deviations for each returned peak. These data were scaled to apparent reflectance ρ_{app} and the sum of all canopy (I_v) and ground (I_g) apparent reflectance values, where ρ_{app} is interpreted as the reflectance of a Lambertian target filling the lidar beam and orthogonal to the pulse direction of travel that would return the same intensity as the actual target (Armston et al., 2013). The ρ_{app} was obtained using the calibration method proposed by Wagner et al. (2006). P_{gap} was then estimated by substituting $I_{v,g}$ for $R_{v,g}$ respectively in Eqs. (9) and (10).

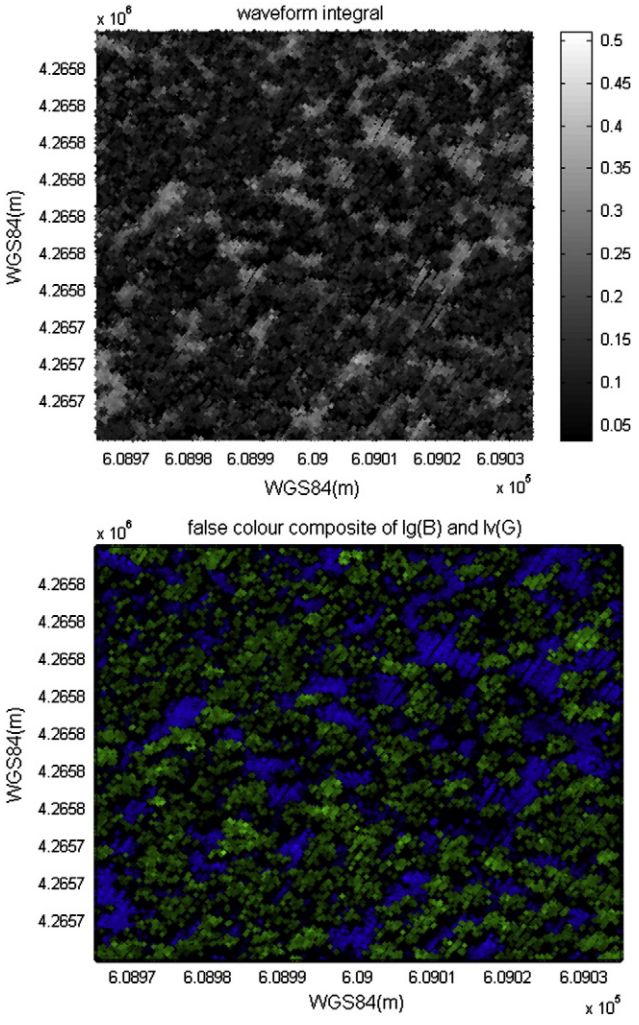

Fig. 8. Spatial variation in canopy and ground backscatter across the test site: total waveform integral (top); false colour composite of the canopy (I_v, green) and ground (I_g, blue) (bottom).

4. Results and discussion

4.1. Relationship between canopy and ground backscatter (I_g and I_v)

Fig. 8 shows spatial images of the total integrals of waveform, including a false colour composite of the corresponding ground (I_g) and canopy (I_v) components. Fig. 8 illustrates the spatial variation in waveform integrals for the test site. Besides the high values of the ground return integrals, Fig. 8 also shows that there are patches of dark ground with similar response to the canopy returns, particularly between the tree crowns (e.g. upper left region). These areas of ground with low ρ_{app} correspond to areas on the forest floor covered mainly with moss. From Fig. 8 it is clear that I_g varies quite strongly across the site.

The distributions of I_v and I_g for pulses that have returns from only the canopy or ground, respectively, are shown in Fig. 9. We see from this that the mean of I_v is consistent with the unimodal spatial distribution of canopy ρ_{app} values in Fig. 8. This supports the assumption of (near) constant ρ_v. Wagner, Hollaus, Briese, and Ducic (2008) also reported similar findings from a dense forest canopy. This is again a very different test of the P_{gap} retrieval method from the sparse tree cover of Armston et al. (2013).

The distributions of I_g shown in Fig. 9 are heterogeneous. The higher relative frequency of lower I_g corresponds to the forest floor covered mainly with moss; higher I_g corresponds to the soil in the marginal areas between the trees, which is consistent with the non-uniform spatial distribution of ground ρ_{app} in Fig. 8.

The relationship between I_g and I_v for individual pulses acquired across the 6 lidar flights and for the original footprint size, is shown in the top left of Fig. 10. The large increase in variance of I_v with decreasing I_g resulted in decreasing linear model fit using the ordinary least squares method due to heteroskedasticity. The small footprint of the lidar data (nearly 0.45 m at 800 m altitude) caused measurements to be very sensitive to high spatial variance in the cross-section and spectral properties of intercepted targets. For I_g, each received waveform may backscatter from an individual moss sward on or near the forest floor or a patch of bare soil between swards. For I_v, each received waveform is likely to be composed of highly variable proportions of needle and woody canopy elements that have different spectral properties at the lidar wavelength of 1550 nm. There are also a few outliers with very high I_v or I_g, due to high apparent reflectance from individual elements reflecting as Fresnel reflectors (Jupp & Lovell, 2007).

For the purpose of reducing local spatial variance and the impact of spatial heterogeneity in the small footprint lidar data, we aggregated all waveforms within a local area and normalised the signal by the number of pulses to simulate a larger footprint waveform (Blair & Hofton, 1999). The remaining three panels in Fig. 10 show the relationship between I_v and I_g using the resulting aggregated pseudo-waveforms created at 2 m, 3 m and 5 m footprint sizes respectively. The least-squares regression fit and resulting Pearson correlation coefficient (R) of all flights I_v and I_g are shown in Fig. 10. For footprint sizes of 5 m for all flights, the variance in I_v is essentially constant with changing I_g. The correlation coefficient $R \geq 0.87$ for all flights, and $R_{average}$ is 0.9. The ratio of ρ_v/ρ_g derived using a footprint size of 5 m for the different flights is stable across different flights at 0.56, 0.57, 0.57, 0.56, 0.55 and 0.55 for flights 1–6 respectively with the largest difference of estimated ρ_v/ρ_g being only 6.3%. We might expect that in cases where canopy cover is much higher (e.g. in dense tropical forests Wagner et al. (2008)) the aggregation scale may need to be larger to ensure adequate ground returns.

It can be seen that the ratio ρ_v/ρ_g is stable i.e. the gradient remains nearly constant across all flights and for all levels of aggregation. This is the single most important piece of evidence supporting the robustness of the P_{gap} retrieval method, relying as it does on the stability of

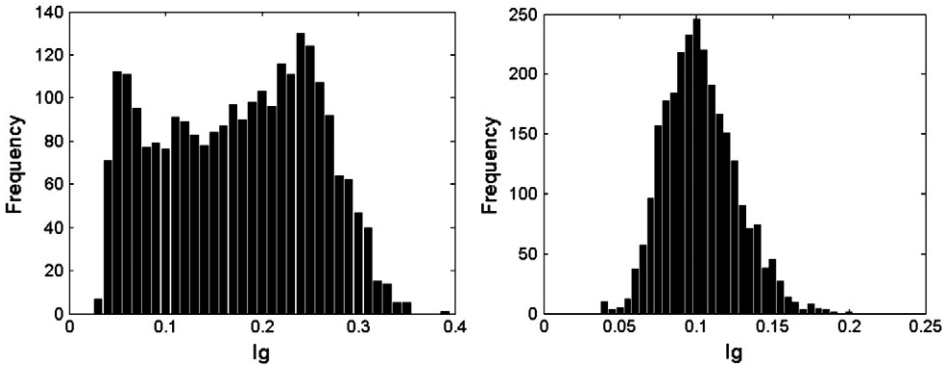

Fig. 9. Histograms of distributions of canopy and ground returns i.e. I_v (left) and I_g (right) for all returns that were identifiable as crown or ground only.

this relationship. There is a small shift in the values from one flightline to another, likely due to the variations in flying height and hence signal-to-noise ratio (SNR) (Goodwin, Coops, & Culvenor, 2006; Morsdorf, Frey, Meier, Itten, & Allgöwer, 2008) as the lines move up in flying height order (see heights in Fig. 4). This result is very encouraging as it would indicate that the method assuming constant ρ_v/ρ_g is likely to be robust to changes of SNR which might occur due to changes in lidar pulse range, instrument gain, or the impacts of slope and scan angle. Instrument gain in particular may vary from flight to flight and may not be known. Here, variation in flying height was small (<50 m) and the instrument gain was known (with internal corrections applied in pre-processing), so changes in SNR likely arose from the impacts of slope and/or scan angle. The strong correlations in Fig. 10 present further evidence that the assumption of stable ρ_v/ρ_g is justified and that it holds across a range of survey and system characteristics.

The change in estimates of ρ_g and ρ_v with footprint (bin) size and different flights are shown in Fig. 11. The estimates of ρ_g and ρ_v stabilise for bin sizes greater than 5 m for all flights, which is consistent with Armston et al. (2013). The estimates of ρ_g and ρ_v calculated as the mean I_g and I_v assuming unimodal ground returns (no spatial aggregation), along with the [0.25, 0.75] quartiles, are also shown in the right side of Fig. 11. This shows that the mean values of I_v are near identical (3.2% average relative error) to the estimates of ρ_v derived by the linear model for bin sizes 5–8 m but the mean values of I_g are slightly biased (8.1% average relative error) compared with estimated ρ_g. This is a key result that supports the assumption made above in Eq. (9) that the integrated canopy returns can be considered Gaussian and unimodal.

4.2. P_{gap} and accuracy assessment

Estimates of P_{gap} derived from the two different lidar methods (full waveform and discrete return HIT) are shown in Fig. 12, plotted against P_{gap} derived from the hemispherical photographs (the mean P_{gap} estimates across 0–5° zenith) described above. We assume that the P_{gap} estimates derived from the hemispherical photos are the actual values, and hence force them to lie on the 1:1 line. The error bars plotted show the mean and variance of all six flights lidar data and hemiphoto-estimated P_{gap} respectively. The waveform-derived estimates of P_{gap} provided the closest match to the hemiphoto estimates, corresponding

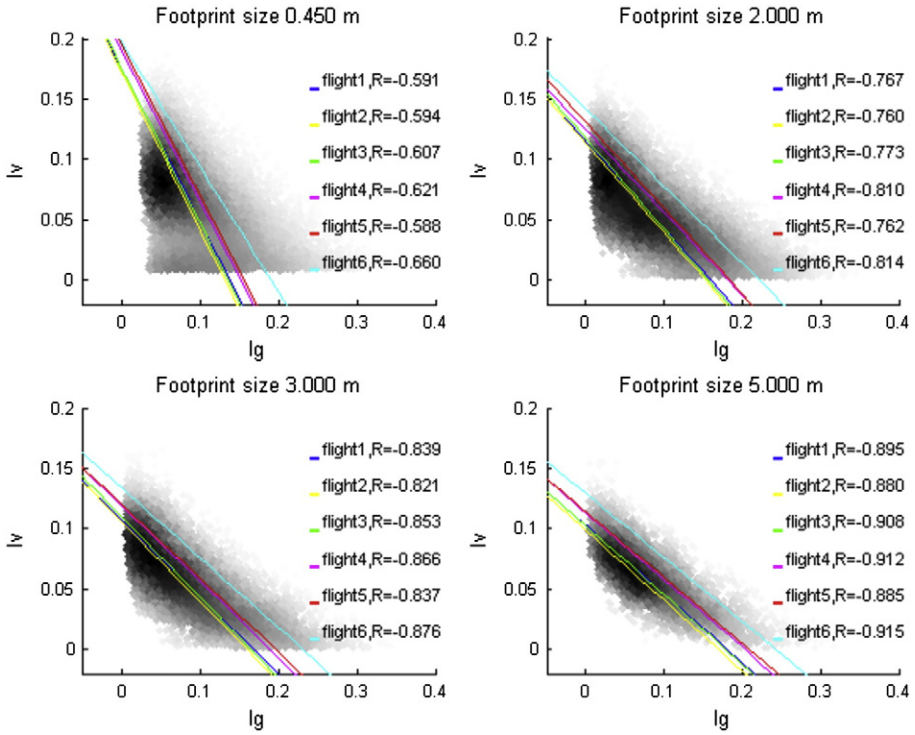

Fig. 10. Scatter plot of the relationships between I_g and I_v for all crown and ground returns with increasing footprint size from the original (top left) of all 6 flights. The estimates of ρ_g and ρ_v derived from this relationship and Pearson correlation coefficient (R) are shown. Darker regions of the scatter indicate a higher density of observations.

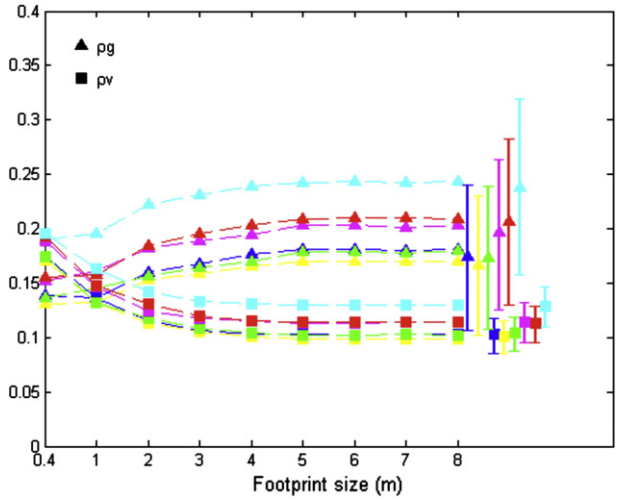

Fig. 11. Values of ρ_g and ρ_v as a function of increasing footprint size. The error bars at higher values represent the mean [0.25, 0.75] quartiles for spatially aggregated footprints. Colours distinguish flight lines as in Fig. 10.

to within 8% and also showing the lowest bias (0.002) and highest correlation ($R = 0.91$). By comparison, the values of P_{gap} derived from the first return HIT method agreed with field measurements to within 14.2% and showed a greater bias. This evidence suggests that the new waveform model of P_{gap} still works with the survey and sensor characteristics shown here. Fig. 12 suggests the lidar-estimated P_{gap}, either from the waveform method or the HIT method, has smaller variance than the hemiphoto estimates, while both have high correlation with the hemiphoto estimates. We note that the hemiphoto data are only for four, spatially-autocorrelated sites; more comparisons are required to establish the robustness of this finding. Differences in $P_{gap}(\theta)$ i.e. directional P_{gap}, for different scan angles account for some of the variance in the lidar-derived estimates.

4.3. Impact of off-nadir scanning angle

The relationships between I_v and I_g across different scan angles from 5 to 30° are shown in Fig. 13. The linear relationship is still strong, even for greater scan angles, with the lowest $R = 0.87$ actually occurring for the angle closest to nadir. The estimates of ρ_v and ρ_g calculated as the mean I_v and I_g of unimodal ground returns (no spatial aggregation) are shown in the right panel of Fig. 13, along with the [0.25, 0.75] quartiles. With the assumption of the same spatial distribution of ground and canopy in different flight lines, there is small variation of ρ_v and the values are nearly identical to the values of mean I_v. This would suggest that for this canopy, the phase function and leaf angle distribution have a relatively small effect, as might be expected due to the small size of needles, oriented in many directions. In addition, the slope in this survey is <9°. Conversely, the estimates of ρ_g decrease with increasing scan angle. This is expected since increasing off-nadir scan angles with increasing lidar beam divergence will, in general, reduce the amplitude of the ground returns (although not the integral unless there is interaction with the instrument SNR threshold) (Yang et al., 2011).

4.4. Impact of slope

There are two areas with different slope angles in the same flight shown in Fig. 14. Excluding the impact of scan angle, the estimates of ρ_v and ρ_g in the nadir scan angle of these two areas in flight 1 are shown in Fig. 15. This illustrates that I_g/I_v is still approximated very well with a linear model even in presence of 26° slope. The estimates of ρ_g and ρ_v calculated as the mean I_g and I_v of unimodal ground returns

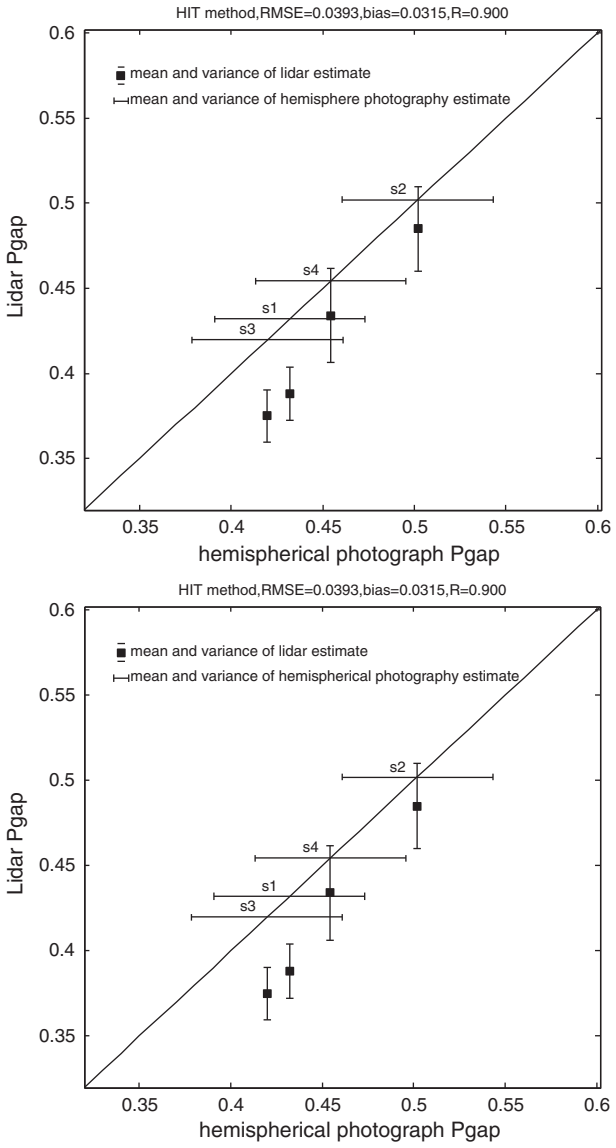

Fig. 12. Estimates of P_{gap} derived from the lidar data using the full waveform returns (top) and synthesised discrete return data (bottom), for each of the six lidar flights. Error bars on lidar-derived P_{gap} arise from variance across all points for each site; those on the hemiphotos arise from variance across all images for each site.

(no spatial aggregation) and the [0.25, 0.75] quartiles are also shown in Fig. 15. These results demonstrate that there is a small decrease of ρ_g with increasing slope which might be caused by projection effects. The values of ρ_v are still very stable with different slopes, and the mean values of I_v are near identical to the estimates of ρ_v derived by the linear model. In cases where off-nadir scan angles occur in the same azimuth direction as steep slopes (e.g. from flights across-slope), the effective scan angle will be increased and so care should be taken to interpret results in these cases. However, the results here suggest that P_{gap} estimates are robust at least up to relative scan angles of ~30°.

These results imply that in this case, the impact of slope on the derivation of P_{gap} is not likely to be large and the I_g/I_v is still approximated very well with a linear model across different off-nadir scan angles and in the presence of quite large slopes. Results also suggest that ρ_v estimated using this model is very stable and nearly identical to the mean value of unimodal canopy return, I_v. This in turn implies that the waveform model can be used to calculate P_{gap} from Eq. (11), just using the mean value of unimodal canopy return I_v. This suggests that the approach could potentially be very flexible across different survey

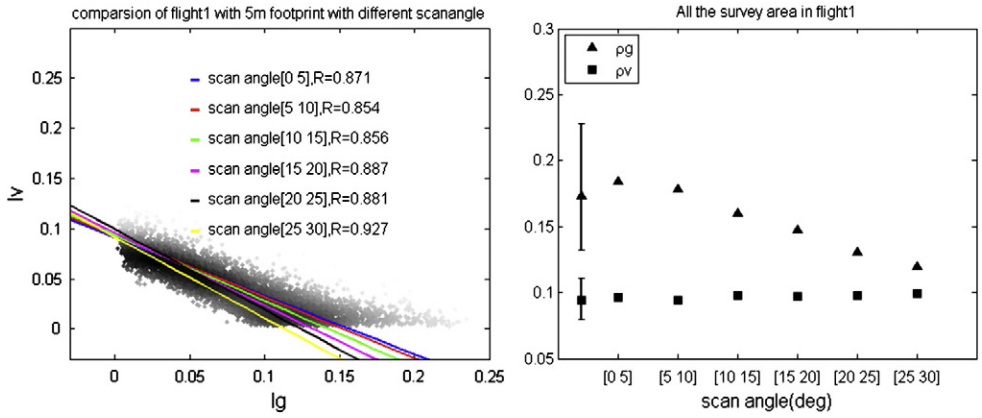

Fig. 13. Relationship between canopy and ground scattering elements, I_v and I_g respectively, as a function of lidar scan angle (left). The grayscale shows the density of points in each region. Also shown (right) are the resulting estimates of estimates of ρ_g and ρ_v along with the mean [0.25, 0.75] quartiles across all flightlines (points with standard deviation as error bars).

situations without fitting Eq. (9), making it potentially very convenient for application in dense forest environments.

5. Conclusions and future work

The aim of this study was to investigate if a newly-proposed method of estimating canopy gap fraction P_{gap} from waveform lidar is robust across varying terrain, canopy and sensor configurations. This method assumes that the ratio of lidar returns from canopy and ground ρ_v/ρ_g is stable, but unlike other methods does not require a priori knowledge of either ρ_g or ρ_v separately, as, crucially, it solves for the ratio ρ_v/ρ_g using the data alone rather than requiring local calibration. We tested this assumption using waveform lidar data over a forested region in China that contains significant canopy, terrain and survey variations, presenting a very different test of the method than previously.

Over a relatively dense forest canopy, the distributions of integrals of ground return I_g were shown to be quite variable. The higher relative frequency of lower values of I_g corresponds to the forest floor which is covered mainly with moss; higher I_g corresponded to the soil in the areas between the trees, which is manifested as spatial variation of

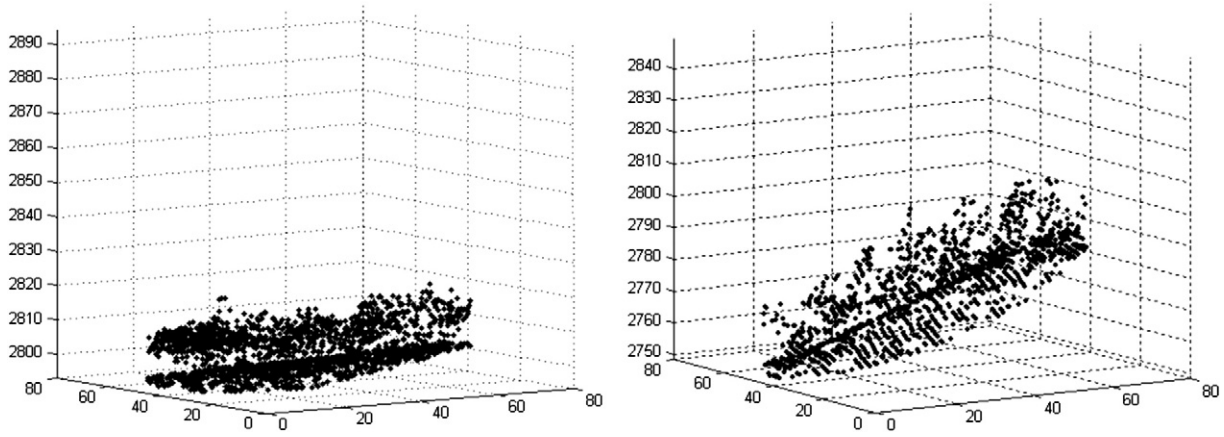

Fig. 14. 3D lidar point cloud showing areas within the lidar datasets with slope ~9° (left panel) and ~26° (right panel).

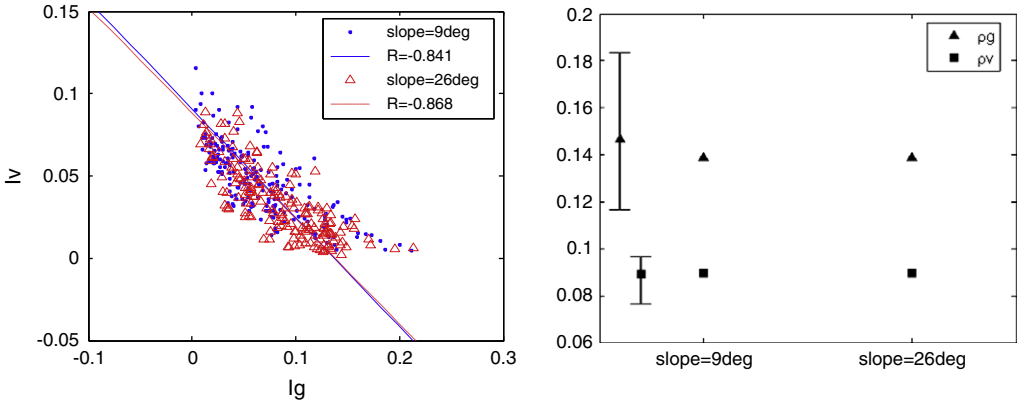

Fig. 15. Variation of I_g and I_v at two different slopes (left panel). The resulting values of mean I_g and I_v for the two cases, including the mean and [0.25, 0.75] quartiles as error bars (right panel).

apparent ground reflectance ρ_{app}. However, the mean values of I_v derived from the waveform data were shown to closely approximate a normal distribution, consistent with the unimodal distribution of canopy apparent reflectance ρ_{app} in dense forest environment. This strongly supports the waveform P_{gap} assumption of constant ρ_v. When spatial variation of footprint returns was minimised by spatially aggregating waveforms to (effective) footprint sizes of 5 m from 0.45 m, the correlation coefficient between I_v and I_g was 0.9 or higher across all flights, resulting in very stable estimates of ρ_v/ρ_g. Different survey configurations (i.e. height, scan angle) were shown to result only in a slight change in offset between the ρ_v/ρ_g, not in the strength of the correlation.

A comparison between P_{gap} estimated from hemiphotos and from the waveform lidar showed close agreement ($R = 0.91$). The waveform P_{gap} agreed to within 8% of the Pgap values derived from hemiphotos, with a bias of 0.17%. In order to compare the waveform P_{gap} method with a method designed for discrete return lidar systems, we synthesised a pseudo-waveform dataset from the discrete return data. We then applied the new P_{gap} estimation method to the resulting pseudo-waveform data in order to test whether it was 'backward compatible' with older sensor systems and datasets. Results showed that the discrete return (HIT)-derived P_{gap} values agreed to within 15% with hemispherical photograph values, with a bias of 3.15%. The discrete return-derived P_{gap} has smaller variance than hemiphoto estimates and has correlation coefficient $R = 0.90$ with P_{gap} derived from hemiphotos. This indicates that while the discrete return data are not as good as the waveform for estimating P_{gap} in this way, they are still useful. This is potentially of considerable practical use given the existence of many discrete return datasets to which this method could be applied retrospectively. Even if estimates of P_{gap} derived in this way were not as good as those from locally-calibrated methods, the fact that local calibration could be avoided, and that assumptions would be consistent across both methods (waveform and discrete return) would be of potential benefit for comparisons over time, or for instances where ground calibration data simply were not available.

In this survey of a dense forest environment, we also tested the impact of lidar system scanning angle and terrain slope on the assumption of constant ρ_v/ρ_g. The new waveform linear model was shown to fit with I_g and I_v across different off-nadir scan angles and in the presence of slopes up to 26° with correlation coefficient $R \geq 0.85$ in all cases. Results also show that ρ_v estimated by the linear model is very stable with different terrain slope angles and scanning angles, yielding values that are almost identical to the mean value of unimodal canopy return, I_v. This means that the waveform model can be used to calculate P_{gap} using just the mean value of unimodal canopy return and I_v. This makes for a very flexible approach, which is robust to choices of site, sensor and survey characteristics and as a result does not rely on local calibrations. This study provides additional evidence that the new method is widely applicable for estimating P_{gap}, and even from discrete return lidar datasets. The method can also be applied to lidar data collected at different times and using different systems, an increasingly important requirement.

Acknowledgements

X. T. Chen's research in UCL was funded by the China Scholarship Council. M. Disney and P. Lewis acknowledge the support of the UK NERC National Centre for Earth Observation (NCEO). We also thank two anonymous reviewers for their detailed and helpful comments.

References

Armston, J., Disney, M. I., Lewis, P., Scarth, P., Phinn, S., Lucas, R., et al. (2013). Direct retrieval of canopy gap probability using airborne waveform lidar. *Remote Sensing of Environment*, *134*(6), 24–38.

Blair, J. B., & Hofton, M.A. (1999). Modeling laser altimeter return waveforms over complex vegetation using high-resolution elevation data. *Geophysical Research Letters*, *26*, 2509–2512.

Campbell, G., & Norman, J. (1989). The description and measurement of plant canopy structure. In R. Russell, B. Marshall, & P. Jarvis (Eds.), *Plant canopies: Their growth, form and function*. : Cambridge University Press.

Chen, E., & Guo, Z. (2008). *WATER: Dataset of forest structure parameter survey at the super site around the Dayekou Guantan forest station.* : Institute of Forest Resource Information Techniques, Chinese Academy of Forestry; Institute of Remote Sensing Applications, Chinese Academy of Sciences. http://dx.doi.org/10.3972/water973.0047.db.

Chen, E., Guo, Z., & Liu, Q. (2008). *WATER: Dataset of forest structure parameter survey at the forest sampling strip around the Dayekou Guantan forest station.* : Institute of Forest Resource Information Techniques, Chinese Academy of Forestry. http://dx.doi.org/10.3972/water973.0053.db.

Disney, M. I., Kalogirou, V., Lewis, P. E., Prieto-Blanco, A., Hancock, S., & Pfeifer, M. (2010). Simulating the impact of discrete-return lidar system and survey characteristics over 2 young conifer and broadleaf forests. *Remote Sensing of Environment*, *114*, 1546–1560.

Goodwin, N., Coops, N., & Culvenor, D. (2006). Assessment of forest structure with airborne LiDAR and the effects of platform altitude. *Remote Sensing of Environment*, *103*(2), 140–152.

Hopkinson, C., & Chasmer, L. (2009). Testing LiDAR models of fractional cover across multiple forest ecozones. *Remote Sensing of Environment*, *113*(1), 275–288.

Jupp, D., & Lovell, J. (2007). *Airborne and ground-based lidar systems for forest measurement: Background and principles*. Tech. rep., CSIRO marine and atmospheric research papers.

Lefsky, M., Hudak, A. T., Cohen, W. B., & Acker, S. A. (2005). Patterns of covariance between forest stand and canopy structure in the Pacific Northwest. *Remote Sensing of Environment*, *95*, 517–531.

Li, X., Li, X. W., Li, Z. X., Ma, M. G., Wang, J., Xiao, Q., et al. (2009). Watershed allied telemetry experimental research. *Journal of Geophysical Research*, *114*, D22103. http://dx.doi.org/10.1029/2008JD011590.

Liu, Q. W. (2009). *Research on the estimation method of forest parameters using airborne LIDAR.* PhD thesis (in Chinese). Beijing, China: Chinese Academy of Forestry.

Liu, J., Melloh, R., Woodcock, C., Davis, R., Painter, T., & McKenzie, C. (2008). Modeling the view angle dependence of gap fractions in forest canopies: Implications for mapping fractional snow cover using optical remote sensing. *Journal of Hydrometeorology*, *9*(5), 1005–1019.

Lovell, J., Jupp, D., Culvenor, D., & Coops, N. (2003). Using airborne and ground-based ranging lidar to measure canopy structure in Australian forests. *Canadian Journal of Remote Sensing*, *29*(5), 607–622.

Morsdorf, F., Frey, O., Meier, E., Itten, K., & Allgöwer, B. (2008). Assessment of the influence of flying altitude and scan angle on biophysical vegetation products derived from airborne laser scanning. *International Journal of Remote Sensing*, *29*(5), 1387–1406.

Ni-Meister, W., Jupp, D., & Dubayah, R. (2001). Modeling lidar waveforms in heterogeneous and discrete canopies. *IEEE Transactions on Geoscience and Remote Sensing*, *39*(9), 1943–1958.

Ni-Meister, W., Lee, S., Strahler, A., Woodcock, C., Schaaf, C., Yao, T., et al. (2010). Assessing general relationships between above-ground biomass and vegetation structure parameters for improved carbon estimate from lidar remote sensing. *Journal of Geophysical Research*, *115*, G00E11.

Pang, Y., Chen, E., Liu, Q., Xiao, Q., Zhong, K., Li, X., et al. (2008). *WATER: Dataset of airborne LiDAR mission at the super site in the Dayekou watershed flight zone on Jun. 23, 2008.* : Institute of Forest Resource Information Techniques, Chinese Academy of Forestry; Institute of Remote Sensing Applications, Chinese Academy of Sciences; Cold and Arid Regions Environmental and Engineering Research Institute, Chinese Academy of Sciences. http://dx.doi.org/10.3972/water973.0220.db.

Riegl (2008). *Software manual: RiANALYZE for Riegl Airborne Laser Scanners LMS-Q560 & LMS-Q680* (5th ed.).

Romanczyk, P., van Aardt, J., Cawse-Nicholson, K., Kelbe, D., McGlinchy, J., & Krause, K. (2013). Assessing the impact of broadleaf tree structure on airborne full-waveform small-footprint LiDAR signals through simulation. *Canadian Journal of Remote Sensing*. http://dx.doi.org/10.5589/m13-015.

Ross, J. (1981). *The radiation regime and architecture of plant stands*. The Hague, Netherlands: Junk Publishers.

Tian, X., Li, Z. Y., van der Tol, C., Su, Z., Li, X., He, Q. S., et al. (2011). Estimating zero-plane displacement height and aerodynamic roughness length using synthesis of LiDAR and SPOT-5 data. *Remote Sensing of Environment*, *115*(9), 2330–2341.

Verstraete, M., Pinty, B., & Myneni, R. (1996). Potential and limitations of information extraction on the terrestrial biosphere from satellite remote sensing. *Remote Sensing of Environment*, *58*(2), 201–214.

Wagner, W., Hollaus, M., Briese, C., & Ducic, V. (2008). 3D vegetation mapping using small-footprint full-waveform airborne laser scanners. *International Journal of Remote Sensing*, *29*(5), 1433–1452.

Wagner, W., Ullrich, A., Ducic, V., Melzer, T., & Studnicka, N. (2006). Gaussian decomposition and calibration of a novel small-footprint full-waveform digitising airborne laser scanner. *ISPRS Journal of Photogrammetry and Remote Sensing*, *60*(2), 100–112.

Yang, W., Ni-Meister, W., & Lee, S. (2011). Assessment of the impacts of surface topography, off-nadir pointing and vegetation structure on vegetation lidar waveforms using an extended geometric optical and radiative transfer model. *Remote Sensing of Environment*, *115*(11), 2810–2822.